CONF-8410220--1

DE85 006125

Conf-8410220--1

RECENT RESULTS FROM THE ANL POLARIZED TARGET GROUP

R. Stanek
Argonne National Laboratory, Argonne, Illinois 60439 USA

Abstract

Results are presented from $\vec{p}\vec{p}$ data which includes spin-spin parameters measured at the ZGS at momenta between 1 and 12 GeV/c, and center-of-mass angles between 8° and 90°. The LAMPF program is reviewed, with data from $\Delta\sigma_L$ and $\Delta\sigma_T$ discussed as well as recent $\vec{n}p$ spin transfer measurements.

I. Introduction

In an attempt to understand the nucleon-nucleon interactions and even further, the nucleon-nucleus interactions, the ideal method is by the construction of the interaction amplitudes. At energies $\lesssim$ 500 MeV, this can rather easily be done by phase shift analyses. At higher energies where many partial waves contribute, the amplitudes must be determined by clever manipulations of the data base parameters. To determine the amplitudes uniquely (to within a phase), at least nine independent parameters at each angle and energy must be measured. However, all the data are not always correct or consistent, so that in reality many more than nine parameters need to be measured. Also, the more parameters constituting the data base, the easier will be the amplitude solution search.

Polarization data have consistently shown many interesting features, including evidence for dibaryons in the spin-spin total cross sections.[1-3] Hence a further motivation for studying spin properties is to thoroughly clarify the dibaryon situation. Although the dibaryon question may always remain unresolved, the experimental data can provide many checks both for models incorporating dibaryons and those which try to explain the observed structures by other mechanisms.

In an attempt to perform the above suggestions for the I=1 system, we will present new data obtained at the ZGS at 12 GeV/c and at 6 GeV/c. This data will include the following for $\vec{p}\vec{p}$ elastic scattering:

12 GeV/c	C_{SS}, C_{SL}	$8° < \theta_{c.m.} < 50°$
	C_{LL}	$8° < \theta_{c.m.} < 90°$
6 GeV/c	K_{ij}, D_{ij}, H_{ijk}	

Also we include some discussions on the low energy data of C_{LL} and C_{SL} between 30° and 50° CM between 1 and 2.5 GeV/c. This data is relevant since it allows us to remark on dibaryon effects in the inelastic cross sections.

We have embarked on a program to investigate the I=0 channel in NN elastic scattering. The np data base has approximately five times less quantity than the corresponding pp case, and the quality is much poorer.[4] We will give a progress report on our experimental program at LAMPF, where our goal is to measure np spin correlation parameters between 40° and 160° CM and at T < 800 MeV. We will also present some of the properties of the LAMPF polarized neutron beam.

II. Definitions

In Fig. 1 we show the definition of the spin directions referred to in elastic scattering. $\hat{N}$ spin direction is normal to the scattering plane and $\hat{L}$ is parallel to the momentum vector of the reacting particles. The $\hat{S}$ direction is defined by $\hat{S} = \hat{N} \times \hat{L}$.

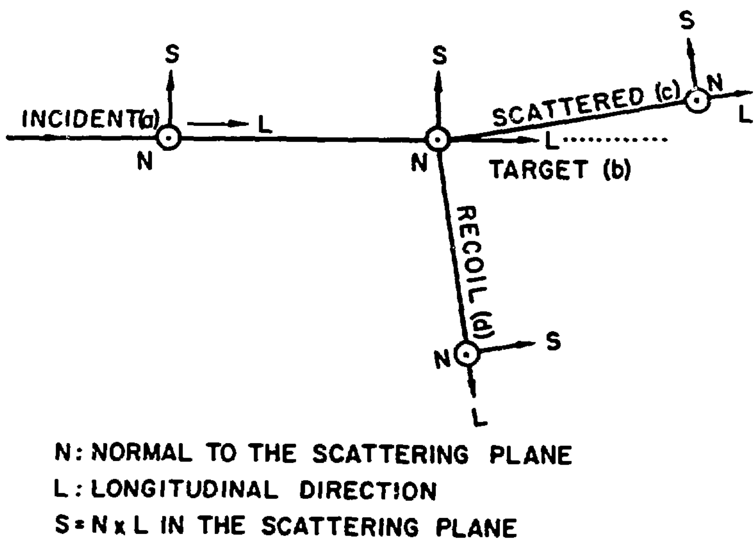

Figure 1 Definitions of the spin direction conventions used in the text.

Table I shows the definitions of the symbols referred to as a function of the experimental spin observables. Here the notation is (Beam, Target; Scattered, Recoil). So, for example, the parameter C_{LL}, the spin correlation coefficient is measured with the beam and target both polarized in the L direction, while the outgoing particles' polarizations are not measured. In other notation, C_{LL} = (L,L;0,0).

Tabl. I

Observable	Description	Symbol
(0,0;0,0)	Differential Cross Section	$d\sigma/d\Omega$
(*,0;0,0) or (0,*;0,0)	Polarization	P
(*,*;0,0)	Correlation Tensor	$C_{jk} = A_{jk}$
(*,0;0,*) or (0,*;*,0)	Polarization Transfer Tensor	K_{jk}
(0,*;0,*) or (*,0;*,0)	Depolarization Tensor	D_{jk}
(*,*;0,*)	Triple Spin Tensor	H_{ijk}
(*,*;*,0)	Triple Spin Tensor	J_{ijk}

For completeness, we present in Table II, the definition of the s-channel helicity amplitudes[5] and their relationships to the t-channel exchange amplitudes.[6] Table III presents the spin observables in terms of the exchange amplitudes.

TABLE II

s-Channel Helicity Amplitudes, $\phi_1 - \phi_5$, and Their Relationship to the Exchange Amplitudes, N_0, N_1, N_2, U_0 and U_2

$\langle ++ \vert ++ \rangle = \phi_1$ $\langle -- \vert ++ \rangle = \phi_2$ $\langle +- \vert +- \rangle = \phi_3$	Net Helicity Non-Flip
$\langle +- \vert -+ \rangle = \phi_4$	Helicity Double-Flip
$\langle ++ \vert +- \rangle = \phi_5$	Helicity Single-Flip

$$N_0 = 1/2\ (\phi_1 + \phi_3)$$

$$N_1 = \phi_5$$

$$N_2 = 1/2(\phi_4 - \phi_2)$$

$$U_0 = 1/2(\phi_1 - \phi_3)$$

$$U_2 = 1/2(\phi_2 + \phi_4)$$

Table III

Laboratory Observables in Terms of Exchange Amplitudes

Observables	(B, T; S, R)	Exchange Amplitudes
(Single Scattering)		
σ^{Tot}		$4\pi/k \; \mathrm{Im} N_0(0)$
$\Delta\sigma_L{}^{Tot}$		$8\pi/k \; \mathrm{Im} U_0(0)$
$\Delta\sigma_T{}^{Tot}$		$-8\pi/k \; \mathrm{Im} U_2(0)$
σ	= (0,0;0,0)	$\lvert N_0\rvert^2 + 2\lvert N_1\rvert^2 + \lvert N_2\rvert^2 + \lvert U_0\rvert^2 + \lvert U_2\rvert^2$
P	= (0,N;0,0) = (N,0;0,0)	$-2\mathrm{Im}\,\{(N_0 - N_2)N_1{}^*\}/\sigma$
C_{NN}	= (N,N;0,0)	$2\mathrm{Re}(U_0U_2{}^* - N_0N_2{}^* + \lvert N_1\rvert^2)/\sigma$
C_{SS}	= (S,S;0,0)	$2\mathrm{Re}(N_0U_2{}^* - N_2U_0{}^*)/\sigma$
C_{SL}	= (S,L;0,0)	$2\mathrm{Re}\{(U_0 + U_2)N_1{}^*\}/\sigma$
C_{LL}	= (L,L;0,0)	$-2\mathrm{Re}(N_0U_0{}^* - N_2U_2{}^*)/\sigma$
Note:	$(d\sigma/dt = \sigma\cdot\pi/k^2)$	
(Double Scattering)		
1. K_{jk} Measurement		
K_{NN}	= (N,0;0,N)	$-2\mathrm{Re}(U_0U_2{}^* + N_0N_2{}^* - \lvert N_1\rvert^2)/\sigma$
K_{SS}	= (S,0;0,S)	$[-2\mathrm{Re}\,\{(U_2-U_0)N_1{}^*\}\sin\theta_R - 2\mathrm{Re}(N_0U_2{}^* + N_2U_0{}^*)\cos\theta_R]/\sigma$
K_{LS}	= (L,0;0,S)	$[-2\mathrm{Re}\,\{(U_2-U_0)N_1{}^*\}\cos\theta_R - 2\mathrm{Re}(N_0U_0{}^* + N_2U_2{}^*)\sin\theta_R]/\sigma$
K_{SL}	= (S,0;0,L)	$[2\mathrm{Re}\,\{(U_2-U_0)N_1{}^*\}\cos\theta_R - 2\mathrm{Re}(N_0U_2{}^* + N_2U_0{}^*)\sin\theta_R]/\sigma$
K_{LL}	= (L,0;0,L)	$[-2\mathrm{Re}\,\{(U_2-U_0)N_1{}^*\}\sin\theta_R + 2\mathrm{Re}(N_0U_0{}^* + N_2U_2{}^*)\cos\theta_R]/\sigma$
2. D_{jk} Measurement		
D_{NN}	= (0,N;0,N)	$\{\lvert N_0\rvert^2 + 2\lvert N_1\rvert^2 + \lvert N_2\rvert^2 - \lvert U_0\rvert^2 - \lvert U_2\rvert^2\}/\sigma$
D_{SS}	= (0,S;0,S)	$[-2\mathrm{Re}\,\{(N_0 + N_2)N_1{}^*\}\sin\theta_R - (\lvert N_0\rvert^2 - \lvert N_2\rvert^2 - \lvert U_0\rvert^2 + \lvert U_2\rvert^2)\cos\theta_R]/\sigma$
D_{LS}	= (0,L;0,S)	$[-2\mathrm{Re}\,\{(N_0 + N_2)N_1{}^*\}\cos\theta_R + (\lvert N_0\rvert^2 - \lvert N_2\rvert^2 + \lvert U_0\rvert^2 - \lvert U_2\rvert^2)\sin\theta_R]/\sigma$
D_{SL}	= (0,S;0,L)	$[2\mathrm{Re}\,\{(N_0 + N_2)N_1{}^*\}\cos\theta_R - (\lvert N_0\rvert^2 - \lvert N_2\rvert^2 - \lvert U_0\rvert^2 + \lvert U_2\rvert^2)\sin\theta_R]/\sigma$
D_{LL}	= (0,L;0,L)	$[-2\mathrm{Re}\{(N_0 + N_2)N_1{}^*\}\sin\theta_R - (\lvert N_0\rvert^2 - \lvert N_2\rvert^2 + \lvert U_0\rvert^2 - \lvert U_2\rvert^2)\cos\theta_R]/\sigma$
3. Three-Spin Measurement		
H_{SSN}	= (S,S;0,N)	$-2\mathrm{Im}\{(U_2 + U_0)N_1{}^*\}/\sigma$
H_{LSN}	= (L,S;0,N)	$2\mathrm{Im}(U_0N_0{}^* - U_2N_2{}^*)/\sigma$
H_{SLN}	= (S,L;0,N)	$-2\mathrm{Im}(N_0U_2{}^* - N_2U_0{}^*)/\sigma$
H_{LLN}	= (L,L;0,N)	$2\mathrm{Im}\{(U_2 + U_0)N_1{}^*\}/\sigma$
H_{SNS}	= (S,N;0,S)	$[2\mathrm{Im}\{(U_2 - U_0)N_1{}^*\}\cos\theta_R + 2\mathrm{Im}(N_0U_2{}^* + N_2U_0{}^*)\sin\theta_R]/\sigma$
H_{LNS}	= (L,N;0,S)	$[-2\mathrm{Im}\{(U_2 - U_0)N_1{}^*\}\sin\theta_R + 2\mathrm{Im}(U_0N_0{}^* + U_2N_2{}^*)\cos\theta_R]/\sigma$
H_{SNL}	= (S,N;0,L)	$[2\mathrm{Im}\{(U_2 - U_0)N_1{}^*\}\sin\theta_R - 2\mathrm{Im}(N_0U_2{}^* + N_2U_0{}^*)\cos\theta_R]/\sigma$
H_{LNL}	= (L,N;0,L)	$[2\mathrm{Im}\{(U_2 - U_0)N_1{}^*\}\cos\theta_R + 2\mathrm{Im}(U_0N_0{}^* + U_2N_2{}^*)\sin\theta_R]/\sigma$
H_{NSS}	= (N,S;0,S)	$[2\mathrm{Im}\{(N_0 + N_2)N_1{}^*\}\cos\theta_R - 2\mathrm{Im}(U_0U_2{}^* - N_0N_2{}^*)\sin\theta_R]/\sigma$
H_{NLS}	= (N,L;0,S)	$[-2\mathrm{Im}\{(N_0 + N_2)N_1{}^*\}\sin\theta_R + 2\mathrm{Im}(U_0U_2{}^* + N_0N_2{}^*)\cos\theta_R]/\sigma$
H_{NSL}	= (N,S;0,L)	$[2\mathrm{Im}\{(N_0 + N_2)N_1{}^*\}\sin\theta_R + 2\mathrm{Im}(U_0U_2{}^* - N_0N_2{}^*)\cos\theta_R]/\sigma$
H_{NLL}	= (N,L;0,L)	$[2\mathrm{Im}\{(N_0 + N_2)N_1{}^*\}\cos\theta_R + 2\mathrm{Im}(U_0U_2{}^* + N_0N_2{}^*)\sin\theta_R]/\sigma$

III. New ZGS Results at 12 GeV/c

We have measured the spin correlation parameters C_{SS} and C_{LS} from between $8° \lesssim \theta_{c.m.} \lesssim 49°$ ($0.2 \lesssim |t| \lesssim 3.5$ GeV/c^2) and C_{LL} from $8° \lesssim \theta_{c.m.} \lesssim 90°$ ($0.2 \lesssim |t|$ 10.2 GeV/c^2) for pp elastic scattering. The experimental apparatus included a recoil proton arm and a forward, large-aperture, magnetic spectrometer. The experimental layout was similar to that shown in Fig. 2.

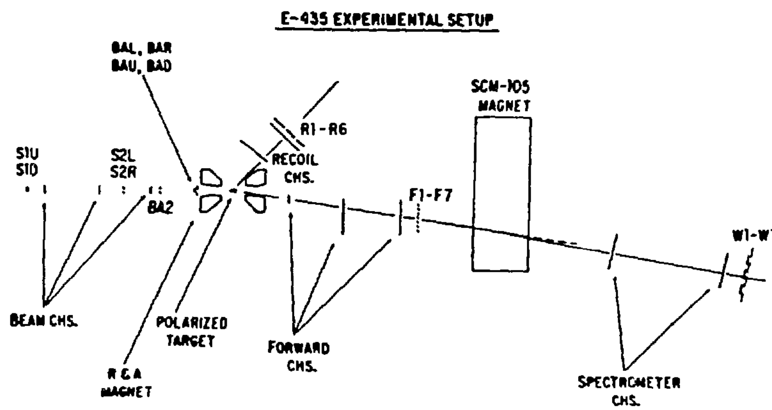

Figure 2 Experimental arrangement for C_{SS} and C_{LS} measurements at 12 GeV/c.

From the five amplitudes,[5]

$$\begin{aligned}
\phi_s &= (\phi_1 - \phi_2)/2 \\
\phi_t &= (\phi_1 + \phi_2)/2 \\
\phi_T &= (\phi_3 - \phi_4)/2 \\
\phi_\tau &= (\phi_3 + \phi_4)/2 \\
\phi_5 &
\end{aligned} \tag{1}$$

we can easily write relationships for the spin correlation parameters. ϕ_s contains only spin singlet terms, ϕ_T and ϕ_τ contain only spin triplet terms, and ϕ_t and ϕ_5 contain only coupled spin triplet terms.

The relationships[7]

$$\begin{aligned}
|\phi_s|^2 &= 1/4(1 - C_{NN} - C_{SS} - C_{LL})d\sigma/d\Omega \\
|\phi_\tau|^2 &= 1/4(1 - C_{NN} + C_{SS} + C_{LL})d\sigma/d\Omega \\
|\phi_t|^2 + |\phi_5|^2 &= 1/4(1 + C_{NN} + C_{SS} - C_{LL})d\sigma/d\Omega \\
|\phi_T|^2 + |\phi_5|^2 &= 1/4(1 + C_{NN} - C_{SS} + C_{LL})d\sigma/d\Omega
\end{aligned} \tag{2}$$

allow us to pursue a model independent amplitude analysis using only the spin correlation parameters, the polarization and the differential cross section. Furthermore, possitivity relations on Eq. 2 yield the inequalities

$$1-|C_{NN} + C_{LL}| > C_{SS} > |C_{NN} - C_{LL}|-1 \qquad (3)$$

At $\theta_{c.m.} = 90°$, the amplitudes ϕ_5 and ϕ_τ vanish,[7] leading to the relationship

$$C_{NN}(90°) - C_{SS}(90°) - C_{LL}(90°) = 1 \qquad (4)$$

At $\theta_{c.m.} \approx 0°$, diffraction dominates pp elastic scattering. In terms of the t-channel helicity amplitudes, the dominant amplitude is[8]

$$\begin{aligned} N_o &= (\phi_1 + \phi_3)/2 \\ &= (\phi_s + \phi_t + \phi_T + \phi_\tau)/2 \end{aligned} \qquad (5)$$

and all other amplitudes are very small. It is therefore expected that $\phi_s \approx \phi_t \approx \phi_T \approx \phi_\tau$. Also $\phi_5 = 0$ at $\theta_{c.m.} = 0$ because of helicity conservation.

In Fig. 3, the square root of the quantities in Eq. 2 are shown. The amplitudes have been normalized such that $d\sigma/d\Omega = 1$. At θ=0, the assumption of N_o dominance allows us to determine the open circles shown in Fig. 3. Also, at 90°, C_{SS} is calculated from Eq. 4, and the results for the quantities at 90° are shown in the figure. At angles other than 90°, limits of the amplitudes were determined and, using these constraints, the dashed line was drawn for the four quantities of Eq. 2.

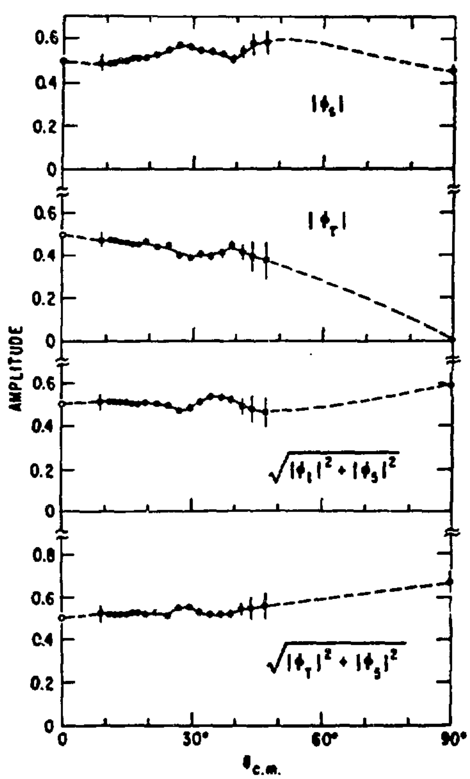

Figure 3 The magnitudes of the quantities expressed by Eq. 2 in the text.

Some structure is seen in all the four quantities in Fig. 3, especially above 25°. We are still in the process of determining the magnitudes of ϕ_t, ϕ_T and ϕ_5 from the data, and these preliminary values will not be presented here.

In Fig. 4a we present the data for C_{SS}, C_{LS} and C_{LL}, and in Fig. 4b show the C_{NN} and polarization data to 90°.[9] The data point shown for C_{SS} at 90° was calculated from the identity at 90° (Eq. 4). The angular dependence of C_{LL} and C_{SS} is seen to be quite different from that of C_{NN}. Both C_{SS} and C_{LL} are consistent with being constant between $40° \lesssim \theta_{c.m.} \lesssim 90°$, while C_{NN} shows rapid changes in this region. Most theoretical models fail to explain these data.[10] However, Anselmino[11] has shown that hard scattering models can work well if the quark recombinations for the final-state protons are correctly treated. Further details on the large angle data can be found in Ref. 12.

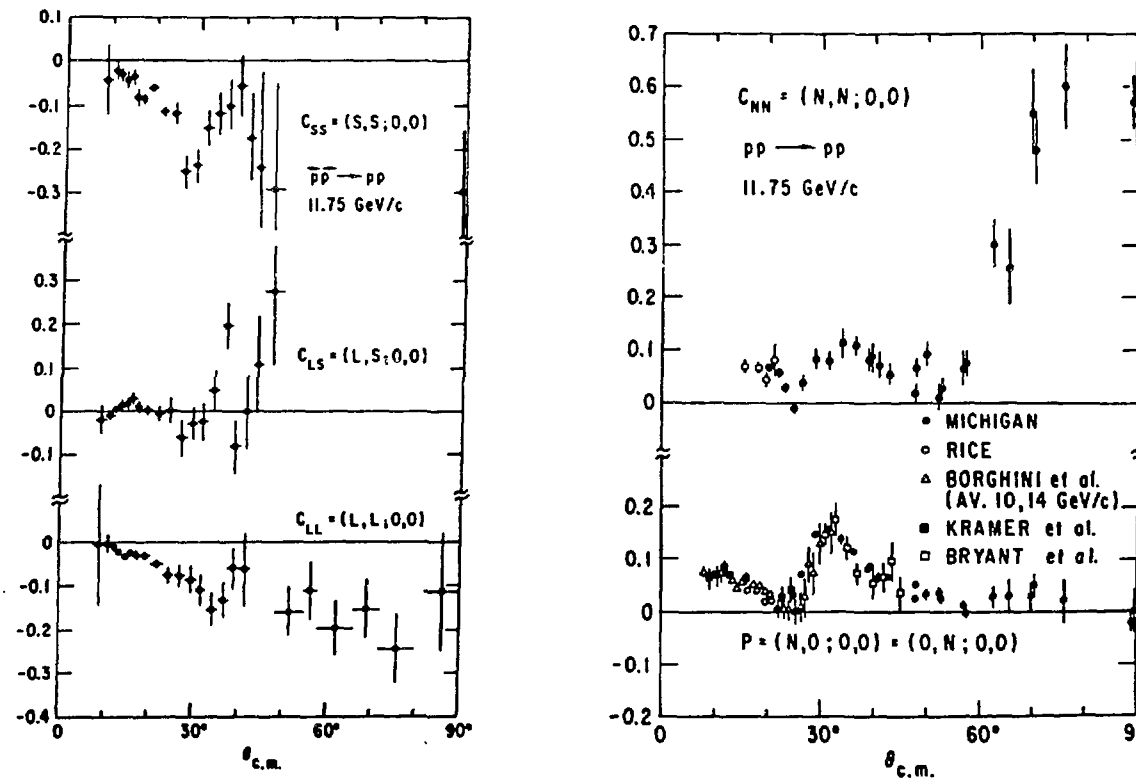

Figure 4 a. The values of C_{SS} and C_{LS} and C_{LL} from the present data. The point for C_{SS} at 90° is derived from Eq. 4.
b. C_{NN} and polarization data.

IV. New ZGS Results at 6 GeV/c

We present results for a variety of two-spin and three-spin correlation parameters for pp elastic scattering in the region of $|t| \lesssim 1$ (GeV/c)^2. This data is important since it brings the total number of pp elastic observables up to fourteen (fifteen if we include $d\sigma/d\Omega$). As mentioned in Section I, we need only nine measurements to determine the amplitudes, but thse additional data together with existing data will enable us to do a completely model-independent amplitude analysis. The abundance of parameters also enables a variety of consistency checks on the data, and there yet exists more data of the present sort under analysis at ANL.

The new data presented here is K_{NN}, K_{LS}, D_{SS}, D_{LS}, H_{NSS} and H_{LNS}. The experimental apparatus is shown in Fig. 5. This detector is similar to that in Fig. 2, but with the addition of a recoil polarimeter. For the calibration of the polarimeter we have used the D_{NN} data from a previous experiment.[13] But because of small differences in the polarimeter, there is some calibration uncertainty in the low -t region.

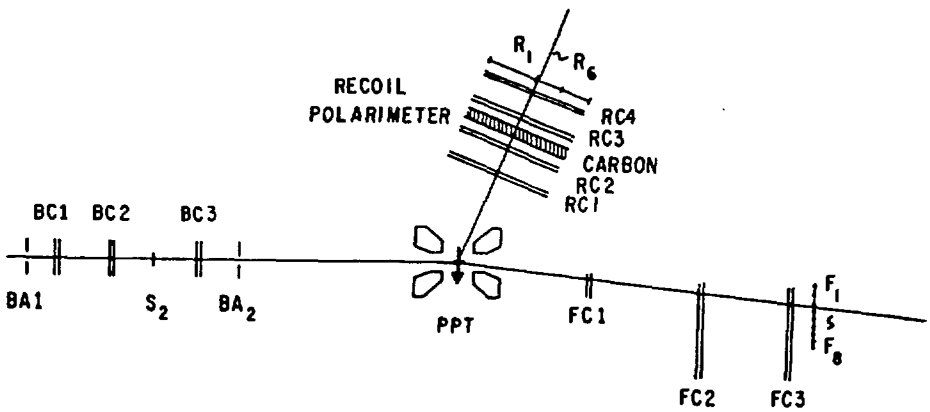

Figure 5 Experimental arrangement for the two-spin and three-spin measurements at 6 GeV/c.

The five paramters, K_{LS}, K_{NN}, D_{SS}, H_{LSN} and H_{NSS} are shown in Fig. 6. At the present time, we feel our data is self-consistent, and consistent with other data as well. Some consistency checks that we have performed are as follows:

- D_{SS} data from Saclay[14] (open circles in Fig. 6) agree within errors with the present data.
- K_{NN} agrees with previous data[15] at $t = -0.5$ $(GeV/c)^2$.
- Assuming N_o dominance, C_{NN}, K_{NN}, C_{LL} and K_{LS} can be expressed in terms of amplitudes as

$$C_{NN} \simeq 2\ \mathrm{Re}(-N_0 N_2^*)/\sigma_0 \simeq -2\ \frac{\mathrm{Im}\ N_2}{|N_0|}$$

$$K_{NN} \simeq -2\ \mathrm{Re}(N_0 N_2^*)/\sigma_0$$

$$C_{LL} \simeq -2\ \frac{\mathrm{Im}\ U_0}{|N_0|}$$

$$K_{LS} \simeq -2\ \frac{\mathrm{Im}\ U_0}{|N_0|}\ \sin\theta_R$$

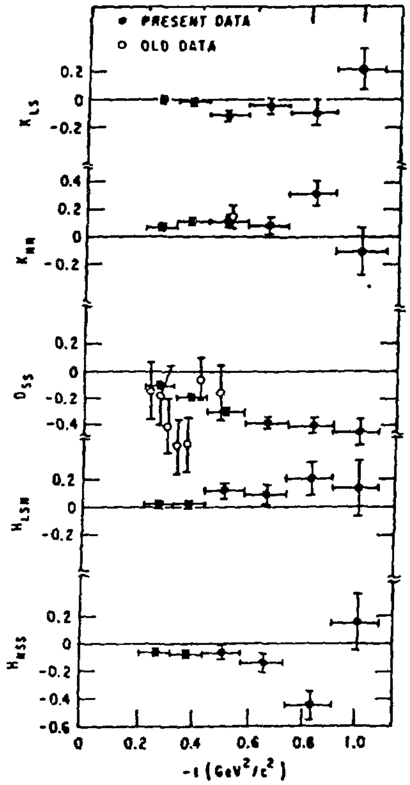

Figure 6 K_{LS}, K_{NN}, D_{SS}, H_{LSN}, data at 6 GeV/c. Also shown are previous measurements for D_{SS} and K_{NN}.

Therefore C_{NN} ≃ and K_{NN} $C_{LL} = K_{LS}/\sin\theta_R$. At $t = -0.38\ (GeV/c)^2$, Miller et al.[15] find $C_{NN} = 0.073 \pm 0.015$. This is to be compared with the present value of $K_{NN} = 0.105 \pm 0.021$. At the same t value, Auer et al.[13,17] find $C_{LL} = -0.018 \pm 0.008$. The present data shows $K_{LS}/\sin\theta_R = -0.011 \pm 0.021$.

Preliminary data for D_{LS} indicate an anomaly. We find at $t = -0.27\ (GeV/c)^2$, $D_{LS} \simeq 30\%$ and at $-t = 0.66$, $D_{LS} \simeq 100\%$. Under the N_0 dominance assumption, we find from Table III that $D_{LS} \simeq 1 \cdot \sin\theta_R$. The D_{LS} data is consistent with other data not yet published. But as of yet, no amplitude solutions have been found with these values for D_{LS}. This may be an indication that the data is incorrect, but it also can mean that the amplitude search has not been very thorough. Another possible explanation for the problem is that there may be a normalization or calibration error with the recoil polarimeter. But so far, the large discrepancies are hard to justify. In any case, a model independent amplitude determination will be completed in about two months.

V. ZGS Results Between 1.2 and 2.5 GeV/c

C_{LL} and C_{SL} have been measured between ~ 30° and ~ 50° in the CM, in the energy range of 1.18 GeV/c to 2.47 GeV/c.[18] The experimental setup is similar to that shown in Fig. 2, with the SCM105 in the forward direction.

The striking energy dependence in $\Delta\sigma_L$ has prompted both experimenters and theorists to further study the NN system.[3] In fact, the existence of dibaryons has been postulated as an explanation of the data, while on the other hand several authors have attempted to explain the data with models not including dibaryon resonances.[19] With the present data at the lower energies, we hope to clarify some of the various interpretations.

In Figs. 7a and 7b we show C_{LL} and C_{SL} and compare the data to two of the existing phase shift predictions.[4,20] Both solutions include dibaryons in the $^1D_2$ and $^3F_3$ states. Both phase shifts show relatively good agreement at $P_{lab} \lesssim 1.5$ GeV/c, but still both solutions have quantitative differences at the higher energies.

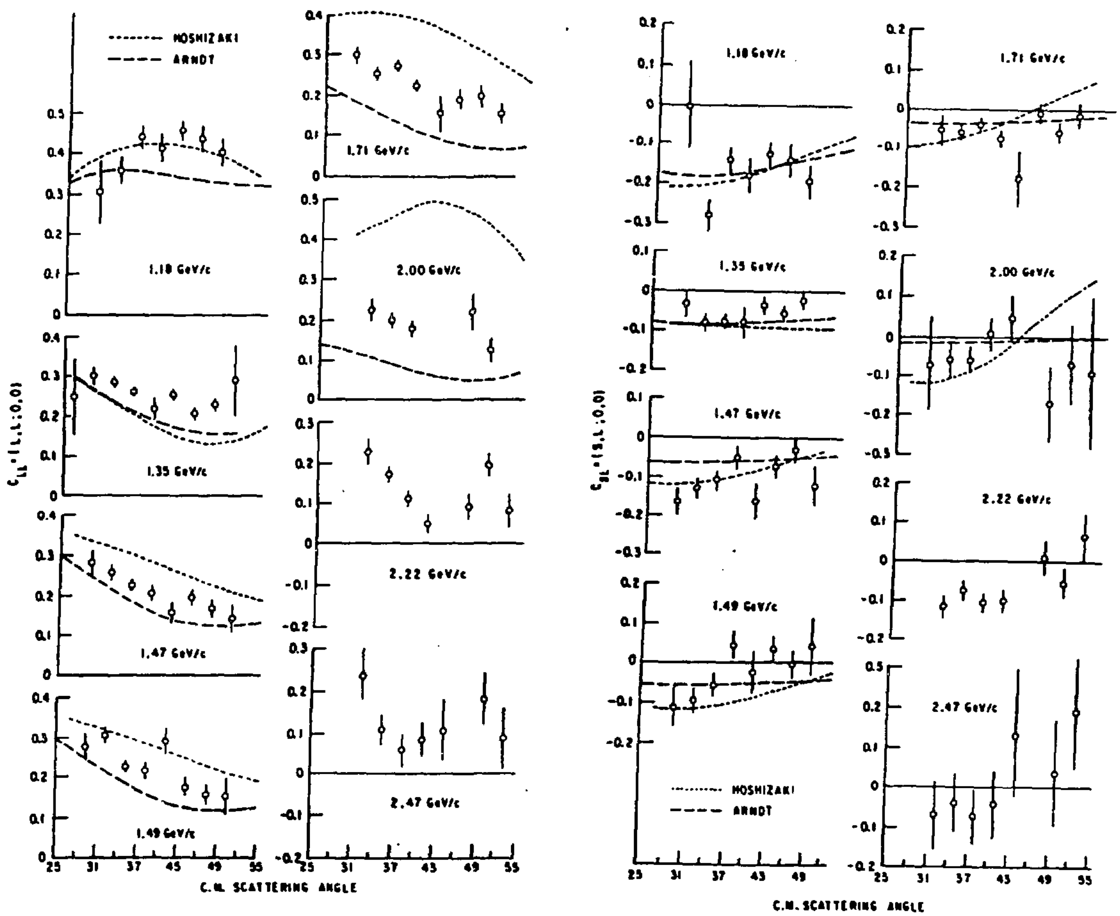

Figure 7 a) The spin-spin correlation parameter C_{LL} together with phase-shift solutions from references 4 and 20.
b) The same for C_{SL}.

The structure in $\Delta\sigma_L$ has been thought to be due to inelastic channels opening. In fact, the dibaryon resonances are known to be highly inelastic.[3,21] Using C_{LL} data, $\Delta\sigma_L$ and dispersion relations, we can calculate $\Delta\sigma_L^{in}$, the inelastic contribution to $\Delta\sigma_L$, and investigate the predictions of the various models. We calculate $\Delta\sigma_L{}^{in}$ from

$$\Delta\sigma_L{}^{in} = \Delta\sigma_L{}^{Tot} - \Delta\sigma_L{}^{elastic}$$

$$\Delta\sigma_L{}^{elastic} = -2 \int d\Omega\ C_{LL}\ (\theta)\ (d\sigma/d\Omega)_{elastic}$$

C_{LL} data from Auer et al.[2] were used for $60° \lesssim \theta_{cm} \lesssim 90^0$ and the present data for $30° \lesssim \theta_{cm} \lesssim 50^0$. Using precise data from σ_{Tot}, $\Delta\sigma_L$ and $\Delta\sigma_T$ by various groups, dispersion theory determines the value of C_{LL} at 0°.[22] $\Delta\sigma_L{}^{elastic}$ is then obtained from the C_o coeficient from the Legendre expansion.

$$C_{LL}\ d\sigma/d\Omega = \sum_{i=0,2,\ldots}^{2\ J_{max}} C_i P_i(\cos\theta)$$

The calculated values of $\Delta\sigma_L{}^{in}$ are shown in Fig. 8 and compared with predictions from models which neglect dibaryon resonances.[23] Also shown are the data from the Geneva group at lower energies for $\Delta\sigma_L(pp \to NN\pi)$.[24] Except at 1.18 and 1.35 GeV/c, the $pp \to \pi d$ channel is negligible and $\Delta\sigma_L{}^{in} = \Delta\sigma_L(pp \to NN\pi)$. At the two lowest energies, the πd channel contributes about 2.9 mb and 1 mb respectively.

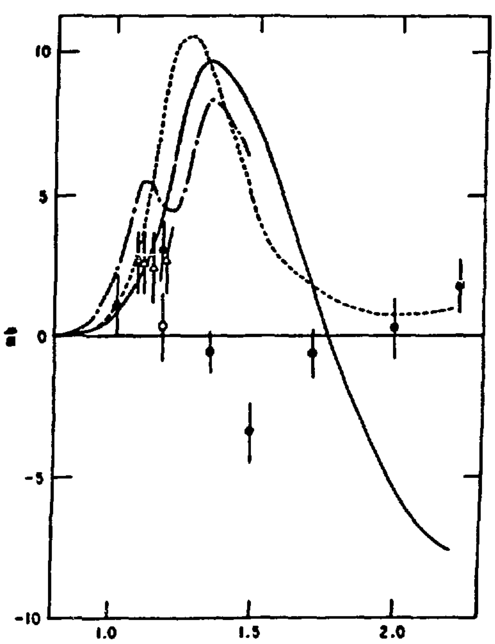

Figure 8 $\Delta\sigma_L{}^{in}$ vs. incident data momentum p_L. ● are the present data, O and Δ are data from Aprile et al., dashed and dot-dashed lines are predictions for $\Delta\sigma_L$ $(pp \to NN\pi)$ from Refs. 23 respectively.

The models based on π-exchange fail except at the very low energies. It seems that the triplet waves, which contribute negatively to $\Delta\sigma_L{}^{in}$, are under estimated. The bump in the predictions at ~ 1.5 GeV/c is similar to the peaks in $\Delta\sigma_T^{Tot}$ and $\Delta\sigma_L^{Tot}$, which are understood as being in the $^1D_2$ wave. We attribute the failure of the π-exchange models to the lack of inclusion of the $^3F_3$ wave. In fact, Kroll, at the Marseilles conference, has pointed out that if he includes the $^3F_3$ in his model, then the curve in Fig. 8 begins to fit the data.

V. Progress at LAMPF

Motivated by the dibaryon questions and the end of the ZGS programs, we have embarked on a program at LAMPF to measure spin observables in the NN elastic system at energies at and below 800 MeV. The pp elastic measurements now completed are $\Delta\sigma_L$, $\Delta\sigma_T$, C_{LL} at 90° and C_{SS} between 20° and 90° in the CM. Our current program is the measurement of the observables in the np elastic channel.

Figure 9 shows the world data of $\Delta\sigma_L$ from the ZGS, SIN, TRIUMF and LAMPF.[1,24-25] The structure is confirmed by all groups, despite normalization discrepancies. In Figure 10 the data for $\Delta\sigma_T$ is shown.[26] Note that the normalization errors between various groups are comparable for $\Delta\sigma_L$ and $\Delta\sigma_T$. We can decompose the cross sections into spin-triplet, σ^T, coupled spin-triplet, σ^t, and spin-singlet, σ^s, cross sections as follows:[27]

$$\sigma^T = \frac{1}{4}(2\sigma^{Tot} - \Delta\sigma_L)$$

$$\sigma^t = \frac{1}{8}\left(2\sigma^{Tot} - 2\Delta\sigma_T + \Delta\sigma_L\right)$$

$$\sigma^s = \frac{1}{8}\left((2\sigma^{Tot} + 2\Delta\sigma_T + \Delta\sigma_L\right)$$

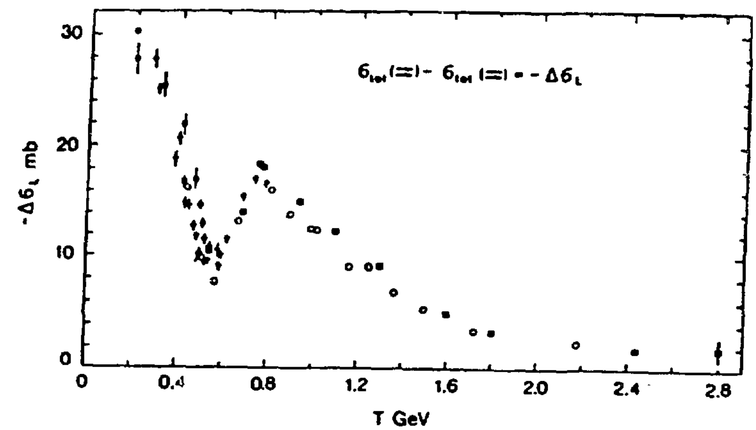

Figure 9
The world data for $\Delta\sigma_L$(np).

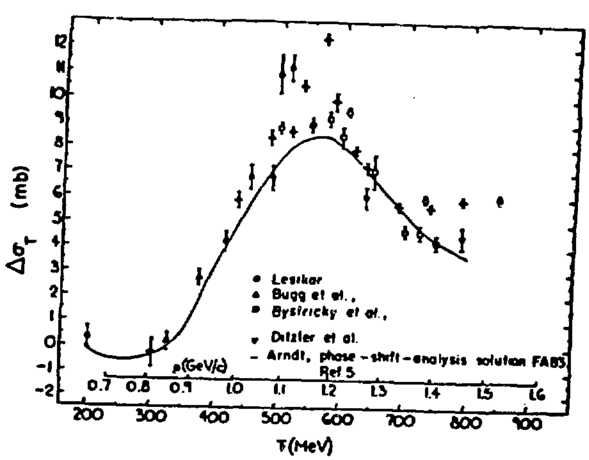

Figure 10 The world data for $\Delta\sigma_T$(np). ● are the measurements of Phillips et al.

Figure 11 shows the three spin cross sections, along with phase shift fits to the data. The individual waves contributing to the phase shifts are also shown. We see that there is clear resonance-like behavior in the $^1D_2$ and $^3F_3$ partial waves. Furthermore, F. Lehar at the Marseilles conference has claimed that the Saclay-Geneva phase shift group has now required that the $^3F_3$ partial wave be resonating. These data and observations certainly add strength to the belief of the existence of dibaryons.

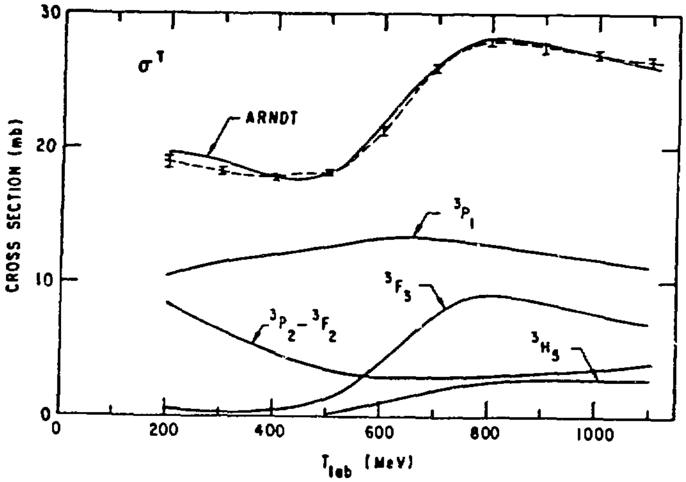

Fig 11a

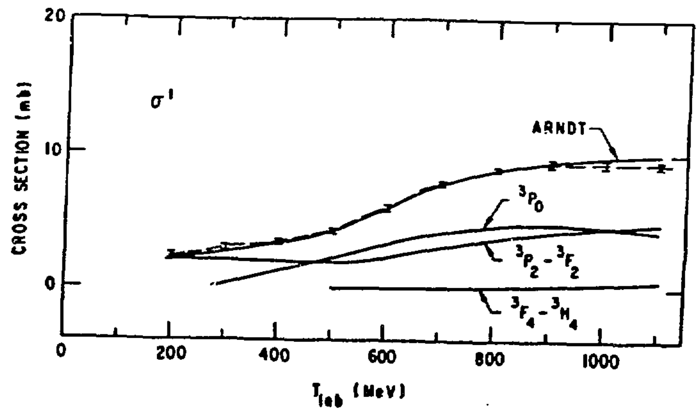

Fig. 11b

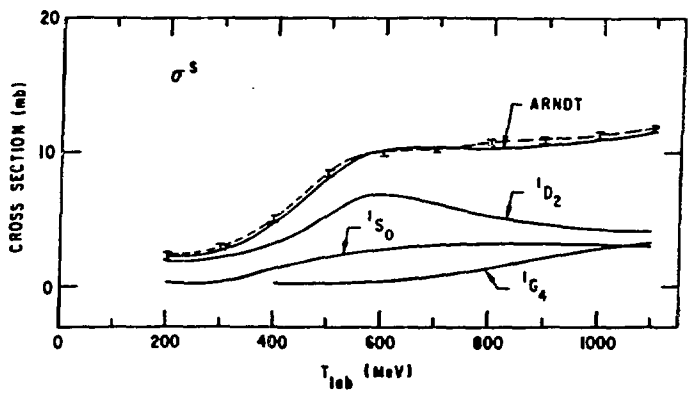

Fig. 11c

Figures 11a, b, c Curves of the three individual spin cross sections, σ^s, σ^t, and σ^T, constructed from the experimental data. Also shown is the Arndt phase shift predictions with the contributions of the various partial waves.

We have also measured C_{LL} at 90° at all the energies $\Delta\sigma_L$ was measured at, and C_{SS} between 20° and 90° at 487, 639 and 791 MeV. These data have been published and we refer the interested reader to the literature.[27-28]

The program we are carrying out to investigate the I=0 channel includes the measurements of many spin correlation parameters for np elastic scattering over a wide range of angles, and at 500, 650 and 800 MeV. Within the next year or so, we will have measurements of C_{SS}, C_{LL}, and C_{LS} between $40° \lesssim \theta_{c.m.} \lesssim 160°$. It can be shown that with the six np observables $d\sigma/d\Omega$, P, C_{LS}, C_{LL}, C_{SS} and C_{NN}-measured at θ and $\pi-\theta$, the I=0 amplitudes can be determined up to eight fold discrete ambiguities.[7,29] These ambiguities may be resolved with further spin observables.

The LAMPF polarized neutron beam is formed from the reaction $\vec{p}d \rightarrow \vec{n}X$ at 0°. Polarized protons are incident on an LD_2 target and the neutrons from the quasielastic reaction, $\vec{p}d \rightarrow \vec{n}pp$, are selected. The beamline is shown in Fig. 12 and the momentum spectra of the neutrons is shown in Fig. 13. There is a clear separation of quasi elastic and inelastic processes. We have measured the neutron polarization at 500, 650 and 800 MeV, and the parameters K_{NN} and K_{LL} are shown in Fig. 14. If the proton spin in the $\hat{L}$ direction is $\vec{P}_{p_L}$ and in the normal direction ($\hat{N}$ or $\hat{S}$) is $\vec{P}_{p_\perp}$, then the magnitude of the neutron spin, $|\vec{P}_n|$, is given by

$$|\vec{P}_n| = \sqrt{|K_{LL}\,\vec{P}_{p_L}|^2 + |K_{NN}\,\vec{P}_{p_\perp}|^2}$$

For protons of 80% polarization, this means we can obtain neutrons of about 40% polarization.

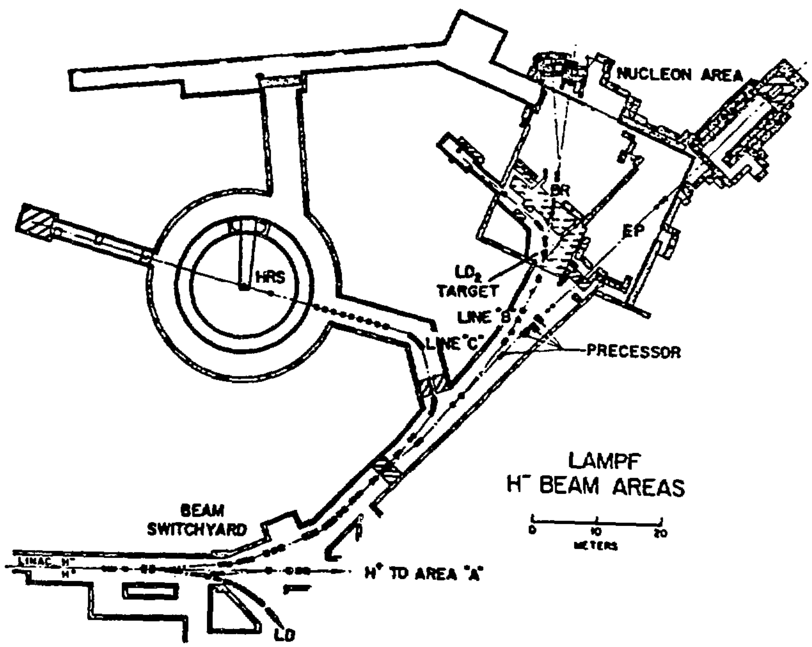

Figure 12

A schematic of the LAMPF beamlines. The neutron experiments are done in area "BR".

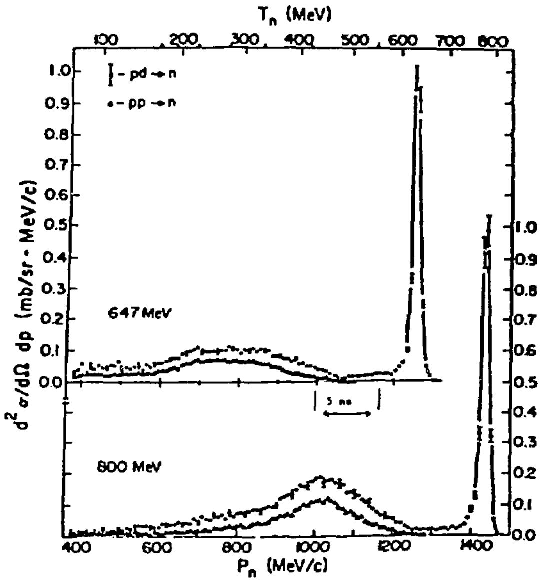

Figure 13 The momenta spectra of the neutrons produced in pd → nX at 0°.

Shown in Fig. 14 is the np → np phase shift predictions by Arndt, as well as the predictions for the quasi-free np scattering.[30] It seems either the phase shifts are wrong, or the correction to the quasi-free scattering may have bad assumptions, which may make the free np parameters difficult to obtain from quasi-free scattering experiments.

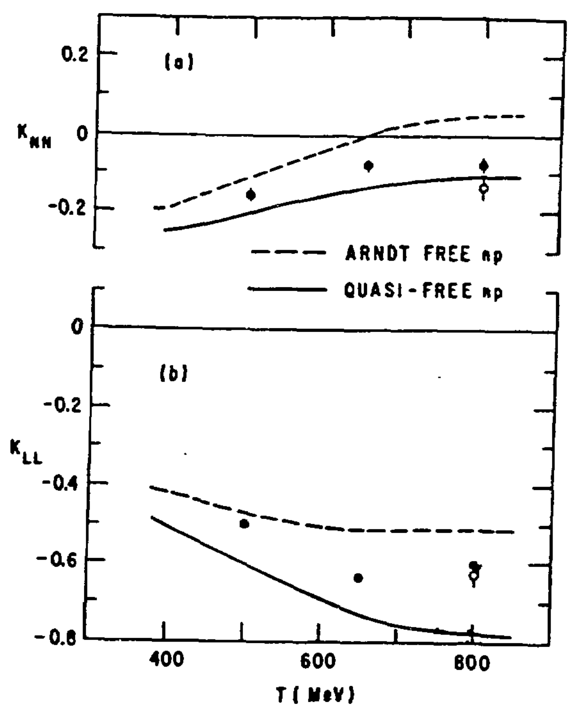

Figure 14

The spin transfer parameters K_{NN} and K_{LL} for the reaction pd → npp at 0°. Also shown are phase shift predictions by Arndt and the quasi-free predictions based on Arndt's phase shifts.

Finally, in Fig. 15 we show the experimental layout for the measurements of the spin-correlation parameters. The polarized neutron beam is precessed to the $\hat{L}$ or $\hat{S}$ direction and impinges on the horizontally polarized target, HERA. The recoil protons are detected in the large aperture spectrometer ($\Delta\theta_{lab} \simeq \pm$

15°), momentum analyzed and the missing mass reconstructed to pick out the elastic events. The analysis of this data is proceeding at a painfully slow pace, and within several months preliminary values for the 500 MeV parameters will be known.

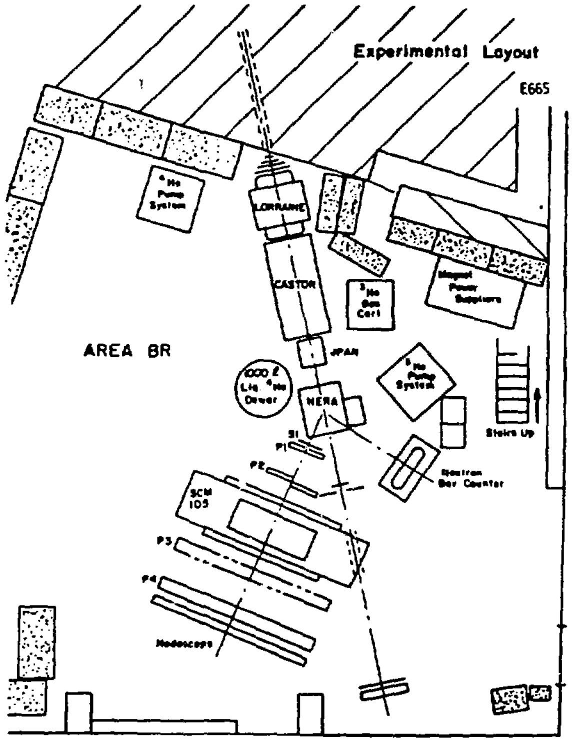

Figure 15 The experimental layout at LAMPF for measuring the spin correlation parameters in np elastic scattering.

REFERENCES

1. I. P. Auer et al., Phys. Rev. Lett. 41, 354 (1978).
2. I. P. Auer et al., Phys. Lett. 67B, 113 (1977); 70B, 475 (1977); Phys. Rev. D24, 2008 (1981).
3. A. Yokosawa, Physics Reports 64, (1980); and references therein.
4. R. A. Arndt et al., Phys. Rev. D28, 97 (1983).
5. M. L. Goldberger et al., Phys. Rev. 120, 2250 (1960); M. Jacob and G. C. Wick, Ann. Phys. (N.Y.) 7, 404 (1979); C. Bourrely et al., Phys. Reports 59, 95 (1980); J. Bystricky et al., J. de Phys. 39, 1 (1978).
6. E. Leader and R. Slansky, Phys. Rev. 148, 1491 (1966); Phys. Rev. 166, 1599 (1968).
7. H. Spinka, Phys. Rev. D30, 1461 (1984).
8. P. Kroll et al., J. Phys. G4, 1003 (1978).
9. K. Abe et al., Phys. Lett. 63B, 239 (1976); H. E. Miettinen et al., Phys. Rev. D16, 549 (1977); M. Borghini et al., Phys. Lett. 24B, 77 (1967); 31B, 405 (1970); 36B, 501 (1971); Bryant et al., Phys. Rev. D13, 1 (1976).

10. C. K. Chen, Phys. Rev. Lett. 41, 1440 (1978); G. R. Farrar et al., Phys. Rev. D20, 202 (1979); S. J. Brodsky et al., Phys. Rev. D20, 2278 (1979); G. Preparata and J. Soffer, Phys. Lett. 86B, 304 (1979).
11. M. Anselmino, Z. Phys. C13, 63 (1982).
12. I. P. Auer et al., Phys. Rev. Lett. 52, 808 (1984).
13. I. P. Auer et al., Phys. Lett. 70B, 475 (1977).
14. J. Deregel et al., Phys. Lett. 43B, 338 (1973); Nucl. Phys. B103, 269 (1976).
15. R. C. Fernow et al., Phys. Lett. 52B, 2431 (1974).
16. D. Miller et al., Phys. Rev. Lett. 36, 763 (1976) and Phys. Rev. D16, 2016 (1977).
17. I. P. Auer et al., Phys. Rev. Lett. 37, 1727 (1976).
18. I. P. Auer et al., Phys. Rev. Lett. 51, 1411 (1983).
19. W. M. Kloet and R. R. Silbar, Phys. Rev. Lett. 45, 970 (1980); W. M. Kloet and J. A. Tjon, Nucl. Phys. A392, 271 (1983); Phys. Rev. C27, 430 (1983).
20. N. Hoshizaki, Prog. Theor. Phys. 61, 129 (1979).
21. J. Bystricky et al., Saclay Report No. DPhPE 82-09, 1982.
22. W. Grein and P. Kroll, Nucl. Phys. A377, 505 (1982).
23. A. König and P. Kroll, Nucl. Phys. A356, 345 (1981); W. M. Kloet and R. R. Silbar, Nucl. Phys. A364, 346 (1981); A. S. Rinat and R. S. Bhalerao, WIS-82/55-Ph., Rehovat (1982).
24. E. Aprile et al., Preprint DPNC, Univ. of Geneva (1983).
25. I. P. Auer et al., Phys. Rev. D24, 2008 (1981); J. P. Stanley et al., Nucl. Phys. A403, 525 (1983); J. Bustricky et al., Phys. Lett. 142, 130 (1984).
26. J. D. Lesikar, Rice Univ. Ph.D. Thesis (1981); D. V. Bugg et al., TRIUMF Annual Report, June 1983; J. Bystricky et al., Saclay note CEA-N-2276, ISSN 0750-6678 (1980-1981); W. R. Ditzler et al., Phys. Rev. D27, 680 (1983); G. Phillips et al., Report LA-10070-PR (1984).
27. I. P. Auer et al., Phys. Rev. D29, 2435 (1984).
28. W. R. Ditzler et al., Phys. Rev. D29, 2135 (1984).
29. L. Puzikov et al., Nucl. Phys. 3, 436 (1957); B. M. Golovin et al., Zh. Eksp. Teor. Fiz. 36, 433 (1959); JETP 9, 302 (1959).
30. R. J. N. Phillips, Proc. Phys. Soc. 74, 652 (1959).

DISCLAIMER